The Astrophysical Journal Letters, 990:L31 (8pp), 2025 September 10 https://doi.org/10.3847/2041-8213/ade6ff
© 2025. The Author(s). Published by the American Astronomical Society.
OPEN ACCESS

ALMA Reveals Bright Circumgalactic Emission and a Biconical Outflow in $z \sim 6.4$ Quasar PSOJ183+05

Manuela Bischetti[1,2], Chiara Feruglio[2,3], Stefano Carniani[4], Valentina D'Odorico[2,3,4], Francesco Salvestrini[2], and Fabrizio Fiore[2,3]

[1] Dipartimento di Fisica, Universitá di Trieste, Sezione di Astronomia, Via G. B. Tiepolo 11, I-34131 Trieste, Italy; manuela.bischetti@units.it, manuela.bischetti@inaf.it
[2] INAF—Osservatorio Astronomico di Trieste, Via G. B. Tiepolo 11, I-34131 Trieste, Italy
[3] IFPU—Institut for Fundamental Physics of the Universe, Via Beirut 2, 34014 Trieste, Italy
[4] Scuola Normale Superiore, Piazza dei Cavalieri 7, I-56126 Pisa, Italy
Received 2025 April 13; revised 2025 June 19; accepted 2025 June 21; published 2025 September 1

Abstract

Understanding gas flows between galaxies and their surrounding circumgalactic medium (CGM) is crucial to unveil the mechanisms regulating galaxy evolution, especially in the early Universe. However, observations of the CGM around massive galaxies at $z > 6$ remain limited, particularly in the cold gas phase. In this work, we present multiconfiguration Atacama Large Millimeter/submillimeter Array (ALMA) observations of [C II]λ158 μm and millimeter continuum emission in the $z \sim 6.4$ quasar PSOJ183+05. We find clumpy [C II] emission, tracing gas up to a $\sim$6 kpc radius, consistent with the interface region between the interstellar medium (ISM) and CGM. The [C II] kinematics shows a rotating disk and a high-velocity, biconical outflow extending up to 5 kpc. The inferred mass outflow rate is $\dot{M}_{\rm of} \sim 930 M_{\odot}\,{\rm yr}^{-1}$, among the highest at $z > 6$, and comparable to the star formation rate. These findings suggest that quasar-driven outflows can rapidly transfer energy and momentum to the CGM, without immediately quenching star formation in the host-galaxy ISM. This supports a delayed feedback scenario, in which outflows reshape CGM conditions and regulate future gas accretion over longer timescales. We find that neither the high-velocity component nor the extended CGM emission in PSOJ183+05 are recovered when using the high-resolution data set alone, which may explain the conflicting results reported regarding [C II] sizes and the detection of outflows at $z \gtrsim 6$. Combining multiconfiguration ALMA data with observations from JWST and the Multi Unit Spectroscopic Explorer will be crucial to map the CGM across its different phases and build a comprehensive picture of the baryon cycle in the first massive galaxies.

Unified Astronomy Thesaurus concepts: High-redshift galaxies (734); Quasars (1319); Emission line galaxies (459); Galaxy evolution (594); Interferometry (808); Circumgalactic medium (1879); Galaxy kinematics (602)

1. Introduction

The acquisition, ejection, and recycling of gas are fundamental processes driving galaxy evolution. The primary site of these gas flows is the circumgalactic medium (CGM), a region extending beyond a galaxy's stellar distribution up to its virial radius and beyond. The CGM serves as a major baryon reservoir, providing inflows of fuel for star formation to the interstellar medium (ISM), and acting as the immediate destination for outflows driven by feedback processes within galaxies (J. Tumlinson et al. 2017). Attaining a complete picture of how galaxies evolve is thus hampered by our incomplete knowledge of the cycle of baryons between the ISM and CGM. This issue is particularly relevant for the first massive ($\gtrsim 10^{10} M_{\odot}$) galaxies, which formed 0.5–1 Gyr after the Big Bang ($z > 6$). According to the hierarchical scenario of structure formation (e.g., V. Springel et al. 2005), these galaxies trace the densest regions of the Universe, which were the first to collapse, and thus represent a relevant population of progenitors of the most massive galaxies that we observe in today's Universe.

The first pioneering studies of CGM halos relied on absorption features of the intervening gas in quasar spectra, and provided a robust description of the average CGM conditions from the first Gyr (e.g., K. L. Adelberger et al. 2005; J. X. Prochaska et al. 2014; M. L. Turner et al. 2014; M. Galbiati et al. 2023; D. Kashino et al. 2023). However, these probes precluded direct constraints on the three-dimensional structure of the CGM. Spatially resolved observations of warm (10^4–10^5 K) CGM emitting gas have been performed with sensitive integral field unit (IFU) spectroscopy using the Multi Unit Spectroscopic Explorer (MUSE). Indeed, CGM halos have been seen routinely glowing in Lyα around massive galaxies hosting quasars up to $z > 6$ (E. Borisova et al. 2016; E. P. Farina et al. 2019). However, millimeter studies (mostly with the Atacama Large Millimeter/submillimeter Array (ALMA)) have so far provided limited statistics on the detection of cold ($\lesssim 10^2$ K) CGM halos around a few massive galaxies and quasars at $z \sim 2$ (C. Cicone et al. 2021; G. C. Jones et al. 2023; J. Scholtz et al. 2023) and at $z > 6$ (C. Cicone et al. 2014; R. A. Meyer et al. 2022; T. S. Lambert et al. 2023; M. Bischetti et al. 2024). Studies based on stacking have also provided conflicting results (S. Fujimoto et al. 2019; M. Novak et al. 2020). This scarcity of detections is likely due to most studies relying on observations not optimized to detect the diffuse CGM gas (e.g., see discussion in S. Carniani et al. 2020).

Different scenarios have been proposed to explain the origin of CGM halos around the first massive galaxies, including stellar and black hole–driven outflows able to push metal-enriched gas to large scales (T. Costa et al. 2022;

Original content from this work may be used under the terms of the Creative Commons Attribution 4.0 licence. Any further distribution of this work must maintain attribution to the author(s) and the title of the work, journal citation and DOI.

E. Pizzati et al. 2023). IFU spectroscopy with the James Webb Space Telescope (JWST) has opened a new window into detecting and mapping warm outflows using the [O III]λ5008 emission line at $z > 6$ (e.g., M. A. Marshall et al. 2023). However, probing outflows in the cold gas phase immediately preceding star formation remains an observational challenge, and only a few detections have been reported (R. Maiolino et al. 2012; C. Feruglio et al. 2017; M. Bischetti et al. 2019a; T. Izumi et al. 2021; R. Tripodi et al. 2022). This is likely due to the limited sensitivity of most millimeter observations, considering similar outflowing to total gas ratios as observed in the low-redshift Universe (M. Bischetti et al. 2019b; A. Fluetsch et al. 2019).

In this work, we present ALMA observations of the [C II] λ158 μm emission line and millimeter continuum emission in the host galaxy of quasar PSOJ183+05 at $z \sim 6.4$ (E. Bañados et al. 2016) and CGM environment. We combined archival observations acquired with different antenna configurations to boost the detectability of diffuse cold gas with respect to previous studies and, at the same time, map it with high angular resolution. The target of this work is a bright quasar with a bolometric luminosity $\log(L_{\rm Bol}/{\rm erg\,s^{-1}}) \simeq 47.2$, powered by a black hole with mass $\log(M_{\rm BH}/M_{\odot}) \simeq 9.4$ and hosting a nuclear wind, as traced by a large blueshift of the C IVλ1549 emission line (E. P. Farina et al. 2022; C. Mazzucchelli et al. 2023). A molecular outflow arising from the central kiloparsec region has been detected in OHλ119 μm absorption by K. M. Butler et al. (2023), with a median velocity of 530 km s^{-1} and an outflow rate of about 75–800$M_{\odot}$ yr^{-1}. Previous [C II] studies of this source reported a bright emission, with a high luminosity $L_{\rm [C\,II]} \simeq 7 \times 10^9 L_{\odot}$ (R. Decarli et al. 2018) associated with a relatively compact disk dominated by rotation (B. P. Venemans et al. 2020; M. Neeleman et al. 2021). Throughout the Letter, we adopt a spatially flat ΛCDM cosmology with $H_0 = 67.4$ km s^{-1}, and $\Omega_M = 0.315$ (Planck Collaboration et al. 2020).

2. ALMA Observations and Data Analysis

We analyze archival ALMA observations of PSOJ183+05 targeting [C II] and band 6 continuum emission using CASA 6.4.0 software (J. P. McMullin et al. 2007). We consider observations of the [C II] $\nu_{\rm rest} = 1900.537$ GHz emission line, as acquired with three different antenna configurations, including a low angular resolution (project ID 2015.1.01115.S, $\sim$1.″1), a high angular resolution (ID 2019.1.01633.S, $\sim$0.″12), and an intermediate resolution (ID 2016.1.00544.S, $\sim$0.″3) data set.

Combining visibilities acquired from different antenna configurations allows us to maximize the sensitivity to possible extended [C II] emission, while keeping a reasonably good angular resolution. We did not combine an additional low-resolution data set (ID 2021.1.01082.S, $\sim$1.″3) available on the archive as its limited spectral coverage (velocities $|v| \lesssim 1000$ km s^{-1}) with respect to the [C II] line would introduce high uncertainty in the modeling and subtraction of the continuum emission.

Visibilities were calibrated using the standard calibration provided by the ALMA observatory and the default phase, bandpass, and flux calibrators. We merged the visibilities from the three data sets using CASA (version 6.6.5) task *concat*. We created a continuum map (Figure 1(a)) by averaging visibilities over all spectral windows, covering the observed frequencies 237.7–242.8 and 252.7–257.9 GHz, and excluding the spectral range covered by [C II]. To model and subtract the continuum emission from the line, we combined the adjacent spectral windows in the baseband containing [C II] and performed a fit in the *uv* plane to channels with $|v| > 1000$ km s^{-1}, using a first-order polynomial continuum. A continuum-subtracted datacube was created using CASA task *tclean*, with the *hogbom* cleaning algorithm in noninteractive mode, a threshold equal to 2 times the rms sensitivity and a natural weighting of the visibilities. We adopted a 30 km s^{-1} channel width. The resulting synthesized beam for the spectral window including [C II] is 0.13×0.12 arcsec^2, the rms sensitivity of the [C II] datacube is $\sigma_{30} = 0.095$ mJy beam^{-1} for a 30 km s^{-1} channel width, and the rms sensitivity of the continuum map is $\sigma_{\rm cont} = 6.6$ μJy beam^{-1}.

We performed a pixel-by-pixel spectral decomposition of [C II] emission detected at $>3\sigma_{30}$ in the continuum-subtracted datacube. To reproduce the [C II] emission line profile in PSOJ183+05 (Figure 1(a)), we considered a model with two Gaussian components: a main one with FWHM < 500 km s^{-1} to account for the systemic [C II] emission, based on previous line width measurements (B. P. Venemans et al. 2020), and a

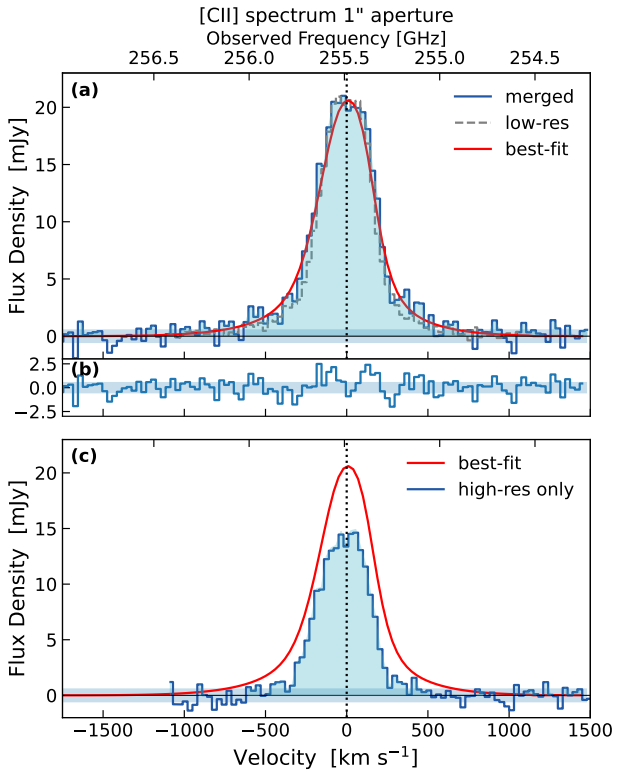

Figure 1. (a) [C II] spectrum extracted from a circular 1″ aperture (blue histogram), similar to the spatial extent of the broad [C II] emission component mapped in Figure 3. The presence of blue/redshifted wings reaching velocities of $\pm$1000 km s^{-1} can be observed. These wings are also present in the spectrum extracted from the same aperture in the low-resolution data set 2021.1.01082.S (normalized for comparison to the peak of the spectrum of the combined data set). The best-fit profile, shown in red, is obtained through a pixel-by-pixel spectral decomposition using a two-Gaussian component model (Section 2). (b) Residual spectrum obtained by subtracting the best-fit model to the data. The horizontal shaded region corresponds to the $\pm1\sigma$ noise level, calculated as $\sigma_{30}\sqrt{N}$, where N is the number of the independent ALMA beams in the extraction aperture. (c) Spectrum extracted from the high-resolution data set alone (Section 2), showing no significant [C II] emission beyond $\pm$500 km s^{-1}.

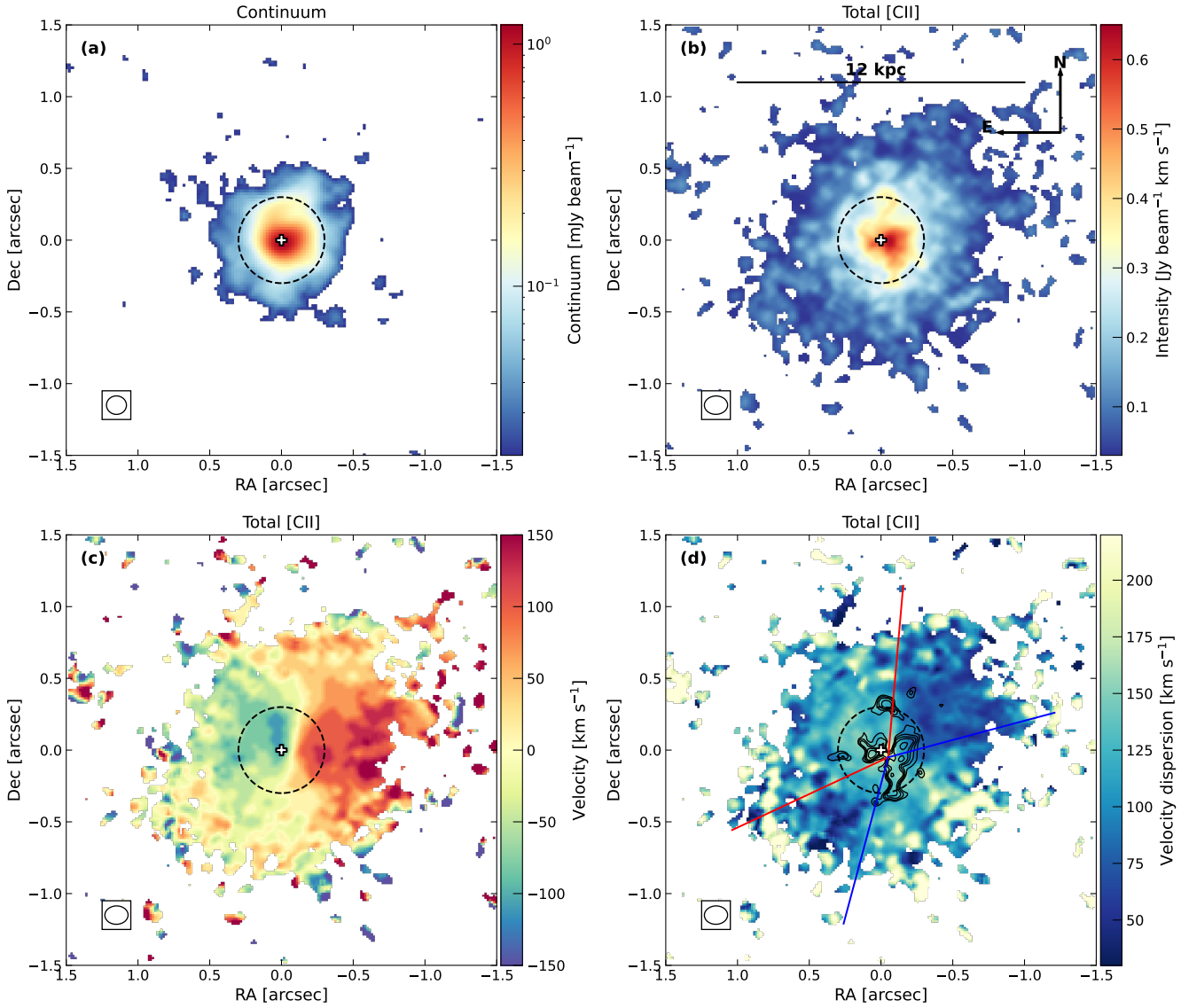

Figure 2. (a) Map of continuum emission detected at $>3\sigma_{\rm cont}$ in the host galaxy of PSOJ183+05. Quasar location, identified as the peak of the ALMA continuum, is shown by the cross. (b) Velocity-integrated intensity map of [C II] emission detected $>3\sigma_{\rm [C\ II]}$. (c) [C II] velocity map. (d) [C II] velocity dispersion map, showing a biconical region oriented along the northeast–southwest direction with high $\sigma_{\rm vel} \sim 150\,{\rm km\,s^{-1}}$, highlighted by the overlaid double cone. Contours highlight the location of the high-velocity [C II] emission with intensity >0.02 Jy beam^{-1} km s^{-1} (Figure 3(a)). The displayed region of 3×3 arcsec^2 corresponds to the field of view covered by JWST/NIRSpec IFU. The dashed circle indicates the size of the stellar distribution measured by JWST/NIRCam observations in the host galaxies of $z \sim 6$ quasars (Section 4.2). The white ellipse shows the ALMA beam.

second broad Gaussian with an FWHM $> 500\,{\rm km\,s^{-1}}$, to account for possible high-velocity wings in the line profile. The amplitude of this broad component is limited at maximum 20% of the systemic component, consistently with the most prominent [C II] wings observed in low-z active galaxies and high-z quasars (R. Maiolino et al. 2012; M. Bischetti et al. 2019a; A. Fluetsch et al. 2019).

The resulting velocity-integrated intensity (0th moment), velocity (1st moment), and velocity dispersion (2nd moment) maps associated with the total [C II] emission in PSOJ183+05 are shown in Figure 2. Moment maps associated with the high-velocity [C II] emission are displayed in Figure 3.

3. Continuum and [C II] Emission

ALMA observations of the ∼240–255 GHz continuum in PSOJ183+05, detected at $\sim 160\sigma_{\rm cont}$ level, reveal that the bulk of the emission is associated with dust in the host-galaxy ISM (Figure 2(a)). By fitting the continuum map with a 2D Gaussian profile, we infer a deconvolved size of $(0.23 \pm 0.01) \times (0.21 \pm 0.01)$ arcsec^2, corresponding to about 1.3×1.2 kpc^2. This compact size is consistent with that previously measured for PSOJ183+05 by B. P. Venemans et al. (2020) using 0.″2 ALMA observations and similar to those reported for the millimeter continuum in the host galaxies of most $z \gtrsim 6$ quasars (e.g., C. Feruglio et al. 2018; R. Tripodi et al. 2024b; F. Salvestrini et al. 2025). It is also consistent with the region in which the bulk of the stellar mass is likely located. Indeed, the dashed circle in Figure 2 corresponds to the effective radius measured by NIRCam on board JWST for the stellar distributions in $z \gtrsim 6$ quasars (e.g., X. Ding et al. 2023; M. A. Stone et al. 2023, 2024; M. Yue et al. 2024), powered by black holes with similar $L_{\rm Bol}$ and $M_{\rm BH}$ to PSOJ183+05.

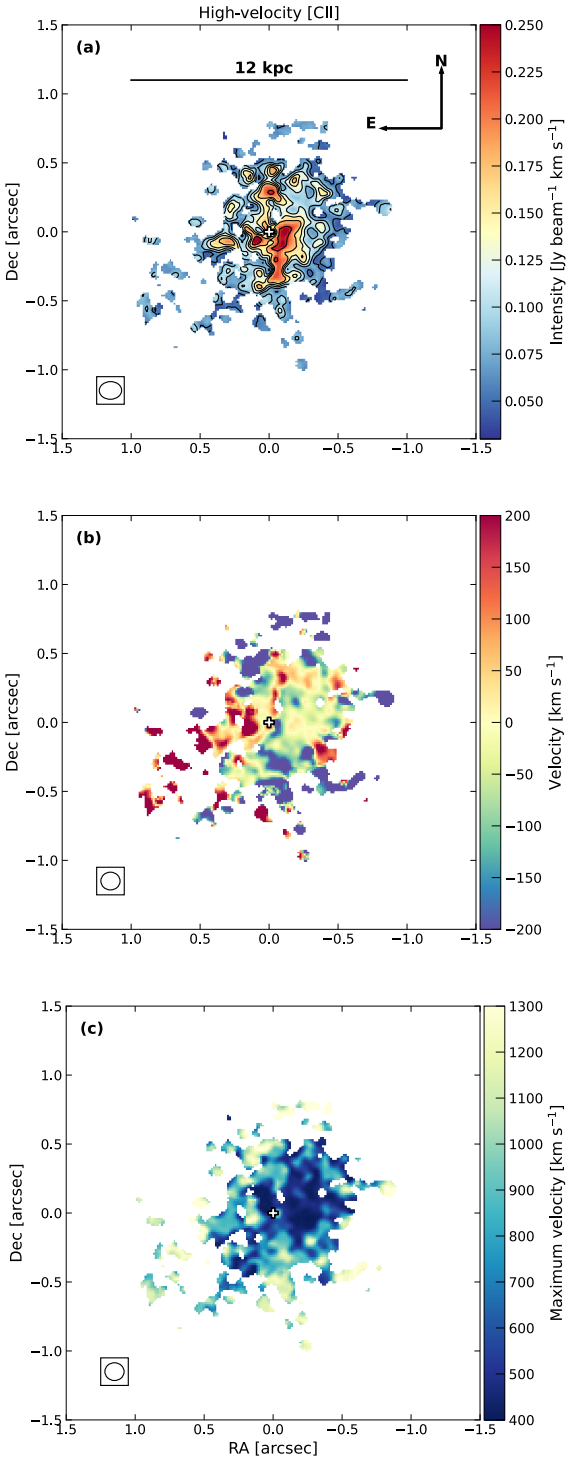

Figure 3. (a) Velocity-integrated intensity map associated with the broad [C II] emission (calculated as in Section 2). Contours correspond to $[2,3,4,5,6,8]\sigma^{\rm of}_{\rm [C\,II]}$. (b) Velocity map. (c) Maximum velocity of the [C II] outflow. The cross refers to the quasar location, corresponding to the peak of the ALMA continuum emission (Figure 2(a)). The white ellipse shows the ALMA beam.

The [C II] emission in PSOJ183+05, detected at $\sim 50\sigma_{\rm [C\,II]}$ level, where $\sigma_{\rm [C\,II]} = 0.015\,{\rm Jy\,beam^{-1}\,km\,s^{-1}}$, spans an angular region of almost $2 \times 2\,{\rm arcsec^2}$ around the quasar location (Figure 2(b)) and appears to be clumpier than the continuum emission (e.g., B. P. Venemans et al. 2019; A. Zanella et al. 2024). We measure a [C II] luminosity (using Equation (1) in P. M. Solomon & P. A. Vanden Bout 2005) $L_{\rm [C\,II]} \simeq 1.1 \times 10^{10} L_{\odot}$ (Table 1), which is a factor of about 2 higher than previous measurements in this source (R. Decarli et al. 2018; B. P. Venemans et al. 2020). By imaging the individual data sets following the approach in Section 2, we verified that this is due to the increased sensitivity to the extended [C II] emission provided by the combined data set (Figure 1(c)). By fitting the [C II] map with a 2D Gaussian profile, we find a deconvolved FWHM size of $(0.83 \pm 0.04) \times (0.75 \pm 0.03)\,{\rm arcsec^2}$, corresponding to about $4.7 \times 4.2\,{\rm kpc^2}$. However, a single component Gaussian fit results in bright residuals (at $\sim 15\sigma_{\rm [C\,II]}$ level, Figure 4(a)) in the central $0\farcs2$ and negative residuals at larger distance from the nucleus, suggesting two distinct [C II] emitting components. No significant residuals are obtained by fitting a two-Gaussian model (Figure 4(b)): this results in a compact component, with a deconvolved major FWHM size of $(0\farcs26 \pm 0.03)$ ($\sim$1.5 kpc), consistent with the continuum size, plus an extended component with an FWHM of $(1\farcs03 \pm 0.04)$, corresponding to about 5.8 kpc. The size of this extended component is a factor of 2 to 3 larger than the [C II] sizes typically measured using high-resolution ($\lesssim 0\farcs2$; M. Bischetti et al. 2018; B. P. Venemans et al. 2020; M. Neeleman et al. 2023) ALMA observations, while it is among the largest sizes reported using moderate or low-resolution ALMA observations, which are more sensitive to [C II] emission on scales $>>1$ kpc (R. Decarli et al. 2018; Y. Fudamoto et al. 2022; F. Wang et al. 2024). The extended [C II] also reaches significantly farther out than the stellar distribution measured by JWST (Figure 2(b)), suggesting that we are probing [C II] emission arising from the interface region between the ISM and CGM.

The [C II] velocity map in PSOJ183+05 (Figure 2(c)) shows a velocity gradient along the east–west direction, consistent with the ISM rotation identified by M. Neeleman et al. (2021), although deviations are present in the northern and mostly in

Table 1
Properties of PSOJ183+0

Parameter	Value
R.A	12:12:26.974
decl.	+05:05:33.540
$z_{\rm [C\,II]}$	6.4388 ± 0.0004
$S_{\rm cont}$ (mJy)	3.53 ± 0.04
$S_{\rm [C\,II]}$ (Jy km s^{-1})	10.10 ± 0.25
$L_{\rm [C\,II]}$ ($10^{10} L_{\odot}$)	1.09 ± 0.03
$M_{\rm atom}$ ($10^{10} M_{\odot}$)	1.51 ± 0.04
[C II] outflow	
$S_{\rm [C\,II]}$ (Jy km s^{-1})	3.64 ± 0.52
$L'_{\rm [C\,II]}$ ($10^{10} L_{\odot}$)	0.39 ± 0.05
$M_{\rm atom}$ ($10^{10} M_{\odot}$)	0.54 ± 0.04
$\langle v_{\rm mom1} \rangle$ (km s^{-1})	-30 ± 65
$\langle v_{\rm max} \rangle$ (km s^{-1})	790 ± 110
$r_{\rm of}$ (kpc)	$0.3 - 4.8$
$\dot{M}_{\rm of}$ ($M_{\odot}$ yr^{-1})	930^{+330}_{-290}

Note. R.A. and decl. refer to the peak of the 237.7–257.9 GHz continuum. $\langle v_{\rm mom1} \rangle$ and $\langle v_{\rm max} \rangle$ are the flux weighted velocity shift and maximum velocity of the outflow, respectively (Figure 3). Uncertainties correspond to a 68% confidence level except for $\dot{M}_{\rm of}$ (see Section 4.1).

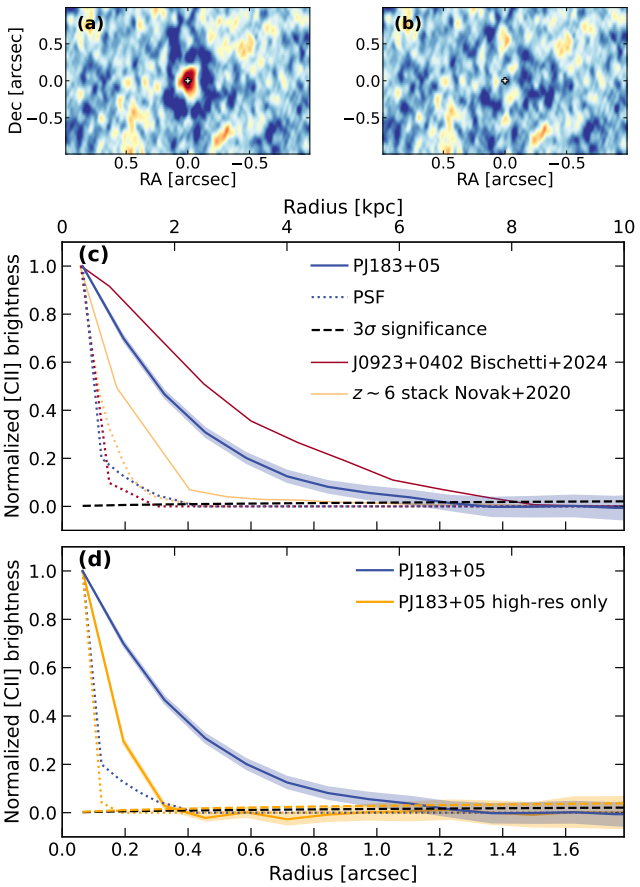

Figure 4. Residual map obtained by fitting a single (a) or a double (b) 2D Gaussian profile to the [C II] 0th moment map (Section 3). (c) Brightness profile of the [C II] emission in PSOJ183+05 (blue solid curve), normalized to the central peak value, and associated 68% confidence level uncertainty (shaded area). The brightness profile associated with the ALMA point-spread function (PSF) is shown by the dotted blue curve, while the dashed curve shows the profile associated with the 3σ level. We also show the profile for another $z \sim 6.6$ quasar (in a merger, red curve) showing extended [C II] emission from M. Bischetti et al. (2024) and the stacked profile of $z \sim 6$ quasar hosts by M. Novak et al. (2020), shown by the yellow curve. (d) [C II] brightness profile of PSOJ183+05 as in panel (c), compared to that extracted from the high-resolution data set alone (Section 2).

the southern regions at ∼3 kpc from the quasar. This may be due to radial gas flows: either inflows close to the minor rotation axis, with a velocity component along the line of sight of $\sim 40\,\mathrm{km\,s^{-1}}$, or outflowing gas whose presence is revealed by high-velocity [C II] emission (Section 4.1). The [C II] velocity dispersion is generally moderate ($\sigma_v \lesssim 100\,\mathrm{km\,s^{-1}}$), consistent with the [C II] clumps being formed through violent disk instabilities, similarly to what is observed in other high-z galaxies and quasars (e.g., S. Inoue et al. 2016; N. M. Förster Schreiber et al. 2018). An increased $\sigma_v \sim 150$–$200\,\mathrm{km\,s^{-1}}$ is observed in a biconical region centered on the quasar and extending out to ∼5 kpc in the northeast to southwest direction. We interpret this increased dispersion as being due to the interaction of a [C II] outflow with the ISM and CGM of the host galaxy (Section 4.1), similarly to what is observed in low-redshift Seyferts and quasars, in which it has been possible to spatially disentangle outflow and disk components (M. Bischetti et al. 2019b; T. T. Shimizu et al. 2019; M. V. Zanchettin et al. 2023). Other processes such as galaxy interactions are disfavored as (i) they cannot reproduce such a symmetric structure with high σ_v (e.g., R. Decarli et al. 2019), and (ii) we do not see a double-peaked continuum or a disturbed [C II] morphology, which suggests that PSOJ183+05 is an isolated galaxy, in agreement with B. P. Venemans et al. (2020) and M. Neeleman et al. (2021). We do not observe a systematic decrease in velocity dispersion with increasing distance from the nucleus.

4. Discussion

4.1. The [C II] Outflow in PSOJ183+05

Figure 3 shows the 0th, 1st, and 2nd moment maps associated with the broad (FWHM $> 500\,\mathrm{km\,s^{-1}}$) [C II] emission detected (at $\sim 8\sigma^{\mathrm{of}}_{[\mathrm{C\,II}]}$ level, where $\sigma^{\mathrm{of}}_{[\mathrm{C\,II}]} = 0.028\,\mathrm{Jy\,beam^{-1}\,km\,s^{-1}}$ is the rms noise of the 0th moment map) in the host galaxy of PSOJ183+05 (Section 2). We find this emission to be very clumpy (Figure 3(a)) and distributed along the edges of the double cone in which the velocity dispersion of the total [C II] profile is increased (Figure 2(d)), out to a distance of ∼5 kpc from the quasar. The velocity shift of this broad component is relatively little ($-200 < v^{\mathrm{broad}}_{\mathrm{mom1}} < 200\,\mathrm{km\,s^{-1}}$), and the emission is mostly redshifted (blueshifted) in the northeast (southwest) cone. We calculate the maximum velocity as $v_{\mathrm{max}} = |v^{\mathrm{broad}}_{\mathrm{mom1}}| + 2\sigma^{\mathrm{broad}}_{v}$ (e.g., M. Bischetti et al. 2017; F. Fiore et al. 2017), where $\sigma^{\mathrm{broad}}_{v}$ is the velocity dispersion of the broad [C II] component. We find that 46% of the gas in the broad component has $v_{\mathrm{max}} > 750\,\mathrm{km\,s^{-1}}$, and 18% reaches v_{max} of ~ 1000–$1200\,\mathrm{km\,s^{-1}}$ (Figure 3(c)). Such velocity is among the highest values measured in the [C II] profiles of local active galactic nuclei and luminous quasars up to $z \gtrsim 6$ (C. Cicone et al. 2014; A. W. Janssen et al. 2016; M. Bischetti et al. 2019a; T. Izumi et al. 2021), and indicates that the broad [C II] emission cannot be ascribed to bounded motion in the quasar host galaxy but is instead associated with outflowing gas. We note that the highest-velocity gas is not detected in the [C II] spectrum extracted from the high-resolution data set alone (Figure 1(c)).

By performing a dynamical modeling of the [C II] kinematics in PSOJ183+05, M. Neeleman et al. (2021) reported a dynamical mass $M_{\mathrm{dyn}} \sim 1.3 \times 10^{11} M_{\odot}$ in the inner 4 kpc around the quasar, which corresponds to an escape velocity of about $700\,\mathrm{km\,s^{-1}}$. This implies that a significant fraction of the high-velocity [C II] emission may be able to escape the potential well of the host galaxy and reach CGM scales if the outflow propagates ballistically. If the outflow is continuously accelerated, even the lower-velocity gas may escape. At the same time, exceeding the local escape velocity may not be a sufficient condition for reaching the CGM if the outflow entrains a large mass, as may be expected for the portion of the outflow cone that propagates into the disk plane (Figure 2(d)).

From the 0th moment map of the high-velocity [C II], we calculate the outflowing atomic gas mass $M_{\mathrm{of}} \sim 5.4 \times 10^{9} M_{\odot}$ in the assumption that most of the [C II] is excited by photodissociation regions, according to Equation (1) in S. Hailey-Dunsheath et al. (2010), for a gas temperature $T = 200$ K and a density significantly higher than [C II] critical density (R. Maiolino et al. 2012; G. Lagache et al. 2018; M. Bischetti et al. 2019a). This value corresponds to about 22% of the total atomic mass in PSOJ183+05. We calculate the mass-outflow rate at each radius r_{of} by applying the relation for a conical wind $\dot{M}_{\mathrm{of}} = \Omega \frac{M_{\mathrm{of}} v_{\mathrm{max}}}{r_{\mathrm{of}}} f$ (e.g., C. Cicone et al. 2015; M. Bischetti et al. 2019b, 2017), where Ω is the fractional solid angle spanned by the outflow bicone, and $f \simeq 1$

for a density profile scaling as $r_{\rm of}^{-2}$, while $f \simeq 3$ for a constant density profile (e.g., F. Fiore et al. 2017; S. Veilleux et al. 2017). In our calculation, we calculate $r_{\rm of}$ for each pixel of the outflow map outside the central beam, while we consider $r_{\rm of}$ equal to the beam radius in the central region. We consider $\Omega \sim 1/2$ (corresponding to a bicone opening angle of about 120°, Figure 2(d)) and $f \simeq 1$. The resulting total atomic mass-outflow rate is $\dot{M}_{\rm of} = 930^{+330}_{-290} M_{\odot}\,{\rm yr}^{-1}$, where the uncertainty is dominated by that on the bicone opening angle (about ±20°). This value is among the highest outflow rates reported in $z \gtrsim 6$ quasars (e.g., R. Tripodi et al. 2024b and references therein). However, it is not much higher than the star formation rate (SFR) ∼650–890$M_{\odot}\,{\rm yr}^{-1}$ measured in the host galaxy of PSOJ183+05 based on multifrequency ALMA data sampling, and assuming a quasar contribution of 50% to dust heating (F. Duras et al. 2017; R. Decarli et al. 2023; R. Tripodi et al. 2024a). This implies that a starburst contribution to the outflow acceleration in PSOJ183+05 cannot be a priori excluded (e.g., M. Bischetti et al. 2019b; A. Fluetsch et al. 2019). However, we calculate an outflow kinetic power $\dot{E}_{\rm of} = \frac{1}{2}\dot{M}_{\rm of} v_{\rm max}^2 \sim 8.3 \times 10^{43}\,{\rm erg\,s}^{-1}$, corresponding to about 0.5% of $L_{\rm Bol}$. This value implies that only a small coupling of the quasar radiation with the host-galaxy medium is sufficient to drive the observed [C II] outflow (T. Costa et al. 2014; A. J. Richings & C.-A. Faucher-Giguère 2018).

A direct comparison between the [C II] outflow and that detected in OH by K. M. Butler et al. (2023) is complicated by the uncertain size of the OH outflow, assumed to be ∼1.2 kpc based on the millimeter continuum. K. M. Butler et al. (2023) also assume a covering factor of unity, providing an upper limit on the molecular mass-outflow rate. Molecular outflows detected in emission, such as those traced by CO, are typically compact, whereas [C II] outflows can reach several kiloparsecs (e.g., C. Cicone et al. 2014; F. Fiore et al. 2017), as observed in PSOJ183+05. As the dynamical timescale inferred from the OH and [C II] outflow is similar (a few Myr), the two phases may trace the same outflow driven by the same black hole accretion or starburst event. In this scenario, the lower OH velocities (500–800 km s^{-1}; K. M. Butler et al. 2023) may be interpreted as denser molecular clumps being embedded in a more diffuse, faster neutral outflow (e.g., A. J. Richings & C.-A. Faucher-Giguère 2018). Accordingly, the total outflow rate could reach ∼2000$M_{\odot}\,{\rm yr}^{-1}$.

The coexistence of powerful winds and high SFR has been often observed in the ISM of high-z quasar host galaxies (C. Feruglio et al. 2017; M. Bischetti et al. 2021; I. Lamperti et al. 2021; A. Vayner et al. 2024) and expected by cosmological simulations of early galaxy evolution (e.g., M. Valentini et al. 2021), which is at odds with the expectations for an ejective feedback mode efficiently removing gas before it can fuel star formation. Instead, recent feedback theories have shifted toward a delayed feedback mode, primarily associated with processes occurring on the CGM scale. The underlying idea is that the physical and kinematic conditions of the CGM may change during the feedback process, and these alterations may be the primary mechanism influencing further gas accretion and, consequently, reducing star formation (P. Barai et al. 2018; T. Costa et al. 2022). Such a scenario may be reasonably applied to PSOJ183+05, as the [C II] wind is able to reach and propagate its energy and momentum to the CGM gas on a short timescale of a few million years, given the observed $v_{\rm max}$.

4.2. Bright CGM Emission and Feedback

The ALMA observations of PSOJ183+05 presented in this work reveal the presence of a bright [C II] emission associated with the host-galaxy ISM and CGM. [C II] is mostly a tracer of neutral atomic gas in photon-dominated regions (PDRs) around young stars, but it can also be emitted from the partly ionized medium (G. Lagache et al. 2018; B. Casavecchia et al. 2024). However, the larger [C II] extent with respect to the millimeter continuum (Figures 2(a),(b)) suggests that a significant fraction of the extended [C II] emission may not arise from PDRs but may rather trace diffuse and ionized gas in the CGM.

This is supported by the fact that about 50% of the [C II] emission arises beyond a radius of 0.″5 (≃2.8 kpc), as can be seen from Figure 2(b) and the [C II] brightness profile of PSOJ183+05 shown in Figure 4(c). The profile shows the average [C II] emission in circular annuli of 0.″13 radius, calculated following the method described in R. Tripodi et al. (2022) and M. Bischetti et al. (2024).

[C II] emission on scales beyond a few kiloparsecs has been previously detected by stacking samples of star-forming galaxies at $z \gtrsim 5$, and in a few individual targets (S. Fujimoto et al. 2019, 2020; M. Ginolfi et al. 2020; R. Herrera-Camus et al. 2021; H. B. Akins et al. 2022; T. S. Lambert et al. 2023). We find that the size of the [C II] emission around PSOJ183+05 is about 2 times more extended than the stacked [C II] profile of $z \sim 6$ quasars by M. Novak et al. (2020). However, we note that the latter profile was based on high-resolution-only observations, which are not optimized to detect possible diffuse [C II] emission. Indeed, by extracting the [C II] brightness profile of PSOJ183+05 from the high-resolution data set alone (Section 2), we find that about 55% of the total [C II] emission and 100% of the emission beyond a 2 kpc radius is not recovered (Figure 4(d)). This is in agreement with ALMA simulated observations of $z > 6$ galaxies by S. Carniani et al. (2020), showing that a major fraction (about 50%) of the flux of the extended [C II] emission is not recovered when employing high-resolution observations only. By combining ALMA observations acquired with different antenna configurations, M. Bischetti et al. (2024) reported the discovery of a bright [C II] emission in the CGM of $z \sim 6.6$ quasar J0923+0402. The size of the [C II] emission in PSOJ183+05 is smaller than that of J0923+0402, although the latter is in a merging system, which might contribute to increasing the region of [C II] emitting gas (M. Ginolfi et al. 2020; T. S. Lambert et al. 2023).

Recent works have suggested a link between feedback and CGM halos around $z \sim 6$ star-forming galaxies and quasars. Given the presence of a large-scale [C II] outflow in PSOJ183+05, such a scenario might explain its extended [C II] emission. Feedback via high-velocity outflows can displace gas beyond a few kiloparsecs (T. Costa et al. 2019; F. Vito et al. 2022), and, at the same time, outflows can significantly contribute to gas heating via shocks (P. N. Appleton et al. 2013; S. Fujimoto et al. 2020; E. Pizzati et al. 2023). The multiphase structure of the CGM gas depends on the fraction of photons reaching the CGM scales, which in turn depends on black hole feedback clearing out the lines of sight (T. Costa et al. 2022). Along the lines of sight with high escape fraction, the halo would be mostly ionized (e.g., P. Barai et al. 2018; A. Obreja et al. 2024), consistent with the Lyα halos frequently detected around high-z quasars (E. Borisova

et al. 2016; E. P. Farina et al. 2019). If the global escape fraction remains relatively low (J. Stern et al. 2021), extended and bright [C II] halos are expected in massive halos such as those of $z \gtrsim 6$ quasars (E. Pizzati et al. 2023; T. Costa 2024).

5. Conclusions

This study has demonstrated that by combining ALMA data sets acquired with different antenna configurations, extended [C II] emission can be detected beyond ISM scale around the host galaxies of $z \gtrsim 6$ quasars. At the same time, mapping the cold gas emission with high resolution allows us to probe the gas kinematics on a broad range of scales ($\sim$500 pc to several kiloparsecs) and to investigate the presence of inflows and outflows and assess their impact on the large-scale gas reservoir. A major fraction of the total [C II] emission is missed when relying on the high-resolution data set alone. This highlights a well-known limitation of interferometric observations in the low-redshift Universe, where galaxies often exhibit large angular sizes compared to the ALMA beam. In such cases, combining multiple array configurations is a commonly adopted strategy (e.g., S. García-Burillo et al. 2021; C. Ramos Almeida et al. 2022). However, this approach has rarely been applied at high redshift (e.g., S. Carniani et al. 2020). Our findings suggest that this limitation may underlie the conflicting results reported in the literature regarding the extent of cold gas reservoirs and the detection of [C II] outflows in high-redshift galaxies (e.g., C. Cicone et al. 2015; M. Bischetti et al. 2019a; M. Novak et al. 2020; R. A. Meyer et al. 2022).

Several quasars and high-z galaxies have already been observed with multiple antenna configurations, which suggests that significant information on the CGM of massive early galaxies lies unexplored in the ALMA archive (e.g., see also M. Bischetti et al. 2024). However, the archival observations contain heterogeneous observations in terms of angular resolution, sensitivity, and frequency coverage, which are not suited for a systematic study of CGM properties. This implies that complementary dedicated ALMA observations are needed.

To build a three-dimensional picture of the multiphase CGM gas, ALMA information can be combined with that provided by MUSE and JWST for the warm ionized gas. In the case of PSOJ183+05, the high redshift implies that Lyα transition lies close to the edge of the MUSE spectral coverage, making a detection of diffuse Lyα more difficult. Indeed, a Lyα CGM halo was not detected in this quasar in a 0.8 hr exposure (E. P. Farina et al. 2019). However, PSOJ183+05 is being followed up with deeper observations as part of the MUSE program 112.262L.002 (PI: E. Farina). In addition, upcoming Cycle 3 JWST observations with NIRSpec IFU (GO program 4912, PI: S. Carniani) will allow us to map the morphology, metal enrichment, and kinematics in the host galaxy and up to the CGM of PSOJ183+05, using rest-frame optical tracers such as H$\alpha\lambda$6564, [O III] λ5008, and other metal lines (M. A. Marshall et al. 2023; R. Decarli et al. 2024; W. Liu et al. 2024). Such an approach is key to building a detailed picture of how baryons cycle between galaxies and their CGM, and improving the current understanding of the evolution of the first massive galaxies.

Acknowledgments

This Letter makes use of the following ALMA data: ADS/JAO.ALMA#2019.1.01633.S (PI: M. Neeleman), ADS/JAO.ALMA#2016.1.00544.S (PI: E. Banados), ADS/JAO.ALMA#2015.1.01115.S (PI: F. Walter), and ADS/JAO.ALMA#2021.1.01082.S (PI: S. Bosman). ALMA is a partnership of ESO (representing its member states), NSF (USA), and NINS (Japan), together with NRC (Canada), MOST and ASIAA (Taiwan), and KASI (Republic of Korea), in cooperation with the Republic of Chile. The Joint ALMA Observatory is operated by ESO, AUI/NRAO, and NAOJ. This work is based in part on observations made with the NASA/ESA/CSA James Webb Space Telescope. The project leading to this publication has received support from ORP, which is funded by the European Union's Horizon 2020 research and innovation program under grant agreement No. 101004719 [ORP]. M.B. acknowledges support from INAF project 1.05.12.04.01—MINI-GRANTS di RSN1 "Mini-feedback" and from UniTs under FVG LR 2/2011 project D55-microgrants23 "Hyper-gal." M.B., C.F., F.F., and F.S. acknowledge support from INAF PRIN 2022 2022TKPB2P "BIG-z," INAF Bando Ricerca Fondamentale 2023 Data grant "ARCHIE," and M4C2 Missione 4 "Istruzione e Ricerca"—Componente C2 Investimento 1.1 Fondo per il Programma Nazionale di Ricerca e Progetti di Rilevante Interesse Nazionale (PRIN) prog. PRIN 2022 PNRR P2022ZLW4T, "Next-generation computing and data technologies to probe the cosmic metal content." F.S. acknowledges financial support from Ricerca Fondamentale INAF 2024 under project "ECHOS" MINI-GRANTS RSN1.

Facility: ALMA.

Software: astropy (Astropy Collaboration et al. 2013, 2018, 2022).

ORCID iDs

Manuela Bischetti https://orcid.org/0000-0002-4314-021X
Chiara Feruglio https://orcid.org/0000-0002-4227-6035
Stefano Carniani https://orcid.org/0000-0002-6719-380X
Valentina D'Odorico https://orcid.org/0000-0003-3693-3091
Francesco Salvestrini https://orcid.org/0000-0003-4751-7421
Fabrizio Fiore https://orcid.org/0000-0002-4031-4157

References

Adelberger, K. L., Steidel, C. C., Pettini, M., et al. 2005, ApJ, 619, 697
Akins, H. B., Fujimoto, S., Finlator, K., et al. 2022, ApJ, 934, 64
Appleton, P. N., Guillard, P., Boulanger, F., et al. 2013, ApJ, 777, 66
Astropy Collaboration, Price-Whelan, A. M., Lim, P. L., et al. 2022, ApJ, 935, 167
Astropy Collaboration, Price-Whelan, A. M., Sipőcz, B. M., et al. 2018, AJ, 156, 123
Astropy Collaboration, Robitaille, T. P., Tollerud, E. J., et al. 2013, A&A, 558, A33
Bañados, E., Venemans, B. P., Decarli, R., et al. 2016, ApJS, 227, 11
Barai, P., Gallerani, S., Pallottini, A., et al. 2018, MNRAS, 473, 4003
Bischetti, M., Choi, H., Fiore, F., et al. 2024, ApJ, 970, 9
Bischetti, M., Feruglio, C., Piconcelli, E., et al. 2021, A&A, 645, A33
Bischetti, M., Maiolino, R., Carniani, S., et al. 2019a, A&A, 630, A59
Bischetti, M., Piconcelli, E., Feruglio, C., et al. 2018, A&A, 617, A82
Bischetti, M., Piconcelli, E., Feruglio, C., et al. 2019b, A&A, 628, A118
Bischetti, M., Piconcelli, E., Vietri, G., et al. 2017, A&A, 598, A122
Borisova, E., Cantalupo, S., Lilly, S. J., et al. 2016, ApJ, 831, 39
Butler, K. M., van der Werf, P. P., Topkaras, T., et al. 2023, ApJ, 949, 122

Carniani, S., Ferrara, A., Maiolino, R., et al. 2020, MNRAS, 499, 5136
Casavecchia, B., Maio, U., Péroux, C., & Ciardi, B. 2024, A&A, 689, A106
Cicone, C., Mainieri, V., Circosta, C., et al. 2021, A&A, 654, L8
Cicone, C., Maiolino, R., Gallerani, S., et al. 2015, A&A, 574, A14
Cicone, C., Maiolino, R., Sturm, E., et al. 2014, A&A, 562, A21
Costa, T. 2024, MNRAS, 531, 930
Costa, T., Arrigoni Battaia, F., Farina, E. P., et al. 2022, MNRAS, 517, 1767
Costa, T., Rosdahl, J., & Kimm, T. 2019, MNRAS, 489, 5181
Costa, T., Sijacki, D., Trenti, M., & Haehnelt, M. G. 2014, MNRAS, 439, 2146
Decarli, R., Dotti, M., Bañados, E., et al. 2019, ApJ, 880, 157
Decarli, R., Loiacono, F., Farina, E. P., et al. 2024, A&A, 689, A219
Decarli, R., Pensabene, A., Diaz-Santos, T., et al. 2023, A&A, 673, A157
Decarli, R., Walter, F., Venemans, B. P., et al. 2018, ApJ, 854, 97
Ding, X., Onoue, M., Silverman, J. D., et al. 2023, Natur, 621, 51
Duras, F., Bongiorno, A., Piconcelli, E., et al. 2017, A&A, 604, A67
Farina, E. P., Arrigoni-Battaia, F., Costa, T., et al. 2019, ApJ, 887, 196
Farina, E. P., Schindler, J.-T., Walter, F., et al. 2022, ApJ, 941, 106
Feruglio, C., Ferrara, A., Bischetti, M., et al. 2017, A&A, 608, A30
Feruglio, C., Fiore, F., Carniani, S., et al. 2018, A&A, 619, A39
Fiore, F., Feruglio, C., Shankar, F., et al. 2017, A&A, 601, A143
Fluetsch, A., Maiolino, R., Carniani, S., et al. 2019, MNRAS, 483, 4586
Förster Schreiber, N. M., Renzini, A., Mancini, C., et al. 2018, ApJS, 238, 21
Fudamoto, Y., Smit, R., Bowler, R. A. A., et al. 2022, ApJ, 934, 144
Fujimoto, S., Ouchi, M., Ferrara, A., et al. 2019, ApJ, 887, 107
Fujimoto, S., Silverman, J. D., Bethermin, M., et al. 2020, ApJ, 900, 1
Galbiati, M., Fumagalli, M., Fossati, M., et al. 2023, MNRAS, 524, 3474
García-Burillo, S., Alonso-Herrero, A., Ramos Almeida, C., et al. 2021, A&A, 652, A98
Ginolfi, M., Jones, G. C., Béthermin, M., et al. 2020, A&A, 643, A7
Hailey-Dunsheath, S., Nikola, T., Stacey, G. J., et al. 2010, ApJL, 714, L162
Herrera-Camus, R., Förster Schreiber, N., Genzel, R., et al. 2021, A&A, 649, A31
Inoue, S., Dekel, A., Mandelker, N., et al. 2016, MNRAS, 456, 2052
Izumi, T., Onoue, M., Matsuoka, Y., et al. 2021, ApJ, 908, 235
Janssen, A. W., Christopher, N., Sturm, E., et al. 2016, ApJ, 822, 43
Jones, G. C., Maiolino, R., Carniani, S., et al. 2023, MNRAS, 522, 275
Kashino, D., Lilly, S. J., Matthee, J., et al. 2023, ApJ, 950, 66
Lagache, G., Cousin, M., & Chatzikos, M. 2018, A&A, 609, A130
Lambert, T. S., Posses, A., Aravena, M., et al. 2023, MNRAS, 518, 3183
Lamperti, I., Harrison, C. M., Mainieri, V., et al. 2021, A&A, 654, A90
Liu, W., Fan, X., Yang, J., et al. 2024, ApJ, 976, 33
Maiolino, R., Gallerani, S., Neri, R., et al. 2012, MNRAS, 425, L66
Marshall, M. A., Perna, M., Willott, C. J., et al. 2023, A&A, 678, A191
Mazzucchelli, C., Bischetti, M., D'Odorico, V., et al. 2023, A&A, 676, A71
McMullin, J. P., Waters, B., Schiebel, D., Young, W., & Golap, K. 2007, in ASP Conf. Ser. 376, Astronomical Data Analysis Software and Systems XVI, ed. R. A. Shaw, F. Hill, & D. J. Bell (San Francisco, CA: ASP), 127
Meyer, R. A., Walter, F., Cicone, C., et al. 2022, ApJ, 927, 152
Neeleman, M., Novak, M., Venemans, B. P., et al. 2021, ApJ, 911, 141
Neeleman, M., Walter, F., Decarli, R., et al. 2023, ApJ, 958, 132
Novak, M., Venemans, B. P., Walter, F., et al. 2020, ApJ, 904, 131
Obreja, A., Arrigoni Battaia, F., Macciò, A. V., & Buck, T. 2024, MNRAS, 527, 8078
Pizzati, E., Ferrara, A., Pallottini, A., et al. 2023, MNRAS, 519, 4608
Planck Collaboration, Aghanim, N., Akrami, Y., et al. 2020, A&A, 641, A6
Prochaska, J. X., Lau, M. W., & Hennawi, J. F. 2014, ApJ, 796, 140
Ramos Almeida, C., Bischetti, M., Garcìa-Burillo, S., et al. 2022, A&A, 658, A155
Richings, A. J., & Faucher-Giguère, C.-A. 2018, MNRAS, 474, 3673
Salvestrini, F., Feruglio, C., Tripodi, R., et al. 2025, A&A, 695, A23
Scholtz, J., Maiolino, R., Jones, G. C., & Carniani, S. 2023, MNRAS, 519, 5246
Shimizu, T. T., Davies, R. I., Lutz, D., et al. 2019, MNRAS, 490, 5860
Solomon, P. M., & Vanden Bout, P. A. 2005, ARA&A, 43, 677
Springel, V., White, S. D. M., Jenkins, A., et al. 2005, Natur, 435, 629
Stern, J., Sternberg, A., Faucher-Giguère, C.-A., et al. 2021, MNRAS, 507, 2869
Stone, M. A., Lyu, J., Rieke, G. H., & Alberts, S. 2023, ApJ, 953, 180
Stone, M. A., Lyu, J., Rieke, G. H., Alberts, S., & Hainline, K. N. 2024, ApJ, 964, 90
Tripodi, R., Feruglio, C., Fiore, F., et al. 2022, A&A, 665, A107
Tripodi, R., Feruglio, C., Fiore, F., et al. 2024a, A&A, 689, A220
Tripodi, R., Scholtz, J., Maiolino, R., et al. 2024b, A&A, 682, A54
Tumlinson, J., Peeples, M. S., & Werk, J. K. 2017, ARA&A, 55, 389
Turner, M. L., Schaye, J., Steidel, C. C., Rudie, G. C., & Strom, A. L. 2014, MNRAS, 445, 794
Valentini, M., Gallerani, S., & Ferrara, A. 2021, MNRAS, 507, 1
Vayner, A., Díaz-Santos, T., Eisenhardt, P. R. M., et al. 2024, arXiv:2412.02862
Veilleux, S., Bolatto, A., Tombesi, F., et al. 2017, ApJ, 843, 18
Venemans, B. P., Neeleman, M., Walter, F., et al. 2019, ApJL, 874, L30
Venemans, B. P., Walter, F., Neeleman, M., et al. 2020, ApJ, 904, 130
Vito, F., Di Mascia, F., Gallerani, S., et al. 2022, MNRAS, 514 1672
Wang, F., Yang, J., Fan, X., et al. 2024, ApJ, 968, 9
Yue, M., Eilers, A.-C., Simcoe, R. A., et al. 2024, ApJ, 966, 176
Zanchettin, M. V., Feruglio, C., Massardi, M., et al. 2023, A&A, 679 A88
Zanella, A., Iani, E., Dessauges-Zavadsky, M., et al. 2024, A&A, 685, A80